

## Author Manuscript

**Title:** Quantitative maps of endosomal DNA processing by single molecule counting

**Authors:** Ved Prakash; Konstantinos Tsekouras, PhD; Muthukumaran Venkatachalapathy, PhD; Laurie Heineke, PhD; Steve Presse; Nils Walter, PhD; Yamuna Krishnan

This is the author manuscript accepted for publication and has undergone full peer review but has not been through the copyediting, typesetting, pagination and proofreading process, which may lead to differences between this version and the Version of Record.

**To be cited as:** 10.1002/ange.201811746

**Link to VoR:** <https://doi.org/10.1002/ange.201811746>

# Quantitative maps of endosomal DNA processing by single molecule counting

Ved Prakash, Konstantinos Tsekouras, Muthukumaran Venkatachalapathy, Laurie Heineke, Steve Pressé, Nils G. Walter\* & Yamuna Krishnan\*

**Abstract:** Extracellular DNA is engulfed by innate immune cells and digested by endosomal DNase II to generate an immune response. Quantitative information on endosomal stage-specific cargo processing is a critical parameter to predict and model the innate immune response. Biochemical assays quantify endosomal processing but lack organelle-specific information, while fluorescence microscopy has provided the latter without the former. Here, we report a single molecule counting method based on fluorescence imaging that quantitatively maps endosomal processing of cargo DNA in innate immune cells with organelle-specific resolution. Our studies reveal that endosomal DNA degradation occurs mainly in lysosomes and was negligible in late endosomes. This methodology is applicable to study cargo processing in diverse endocytic pathways and measure stage-specific activity of processing factors in endosomes.

Macrophages are innate immune cells that endocytose single- and double-stranded DNA through scavenger receptors. Endocytosed DNA cargo is trafficked along the endolysosomal pathway, progressing from the early endosome to the late endosome, finally reaching the lysosome where it is degraded. The stage-specific processing

of endocytic cargo has important implications for pathogen evasion of the immune system, antigen cross-presentation, as well as in differentiating “self” i.e., molecules of host origin, and non-self i.e., molecules of foreign or pathogenic origin (1–3). DNA is distinguished as self or non-self by host immune cells based on their relative rates of digestion in endocytic organelles (2). Immunogenic CpG containing DNA (CpG-DNA) is processed in endolysosomes of dendritic cells by DNase II such that the digestion-resistant DNA fragments activate Toll like receptor-9 (TLR-9) (4). However, it is still unclear in which organelle these processes occur due to the paucity of quantitative assays in cargo processing while retaining organelle-specific localization information. Endosomal processing is mainly studied using biochemical assays such as sulfation, radio labeling, RT-PCR and transient or induced protein expression.(5–8) While these methods quantitate cargo processing in cell extracts lacking organelle-specific spatial information cannot be obtained. In contrast, fluorescence microscopy provides organelle-specific spatial information but without the ability to quantitate endocytosed cargo (5,9,11,12,30). Although super-resolution microscopy has been used to quantitate marker proteins in organelles,(13,14) one still cannot quantitatively map the processing of endocytic cargo.

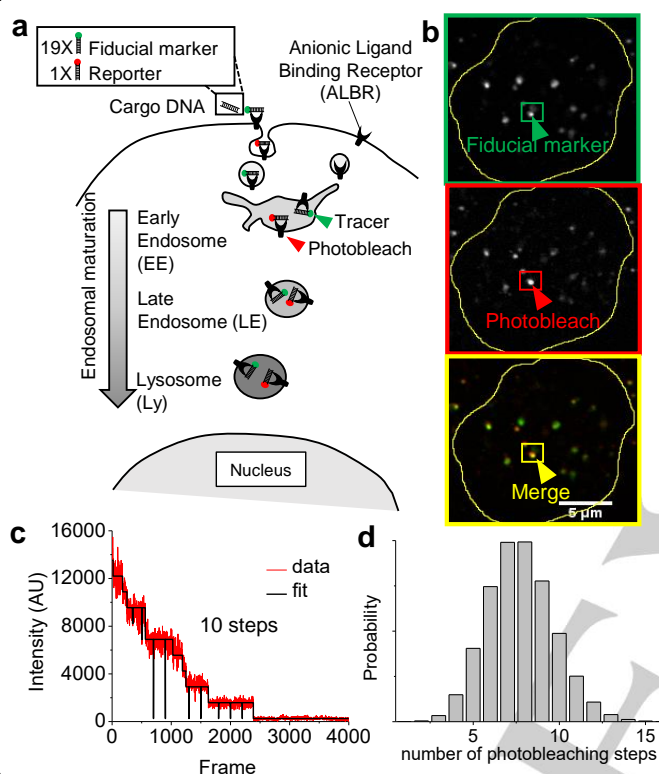
Here, we have developed a method to count endosomal cargo by photobleaching by targeting fluorescently labeled DNA to specific subcellular compartments (15). Photobleaching has been used to count cytosolic microRNA copy number (16). Here, we expand this concept to include organelle-specific information and thereby address cargo processing by developing a method called organellar single-molecule, high-resolution localization and counting (oSHiRLoC). Using

[a] Dr. Laurie Heineke and Prof. Nils G. Walter\*  
Single Molecule Analysis Group, Department of Chemistry,  
University of Michigan, Ann Arbor, MI 48109-1055, USA  
[nwalter@umich.edu](mailto:nwalter@umich.edu)

[b] Dr. Ved Prakash<sup>1</sup>, Dr. Muthukumaran Venkatachalapathy<sup>1</sup> and  
Prof. Yamuna Krishnan<sup>1,2,\*</sup>  
<sup>1</sup>Department of Chemistry, University of Chicago, Chicago, Illinois  
60637, USA and <sup>2</sup>Grossman Institute of Neuroscience, Quantitative  
Biology and Human Behavior, Univ of Chicago, Chicago, Illinois,  
60637, USA  
[yamuna@uchicago.edu](mailto:yamuna@uchicago.edu)

[c] Dr. Konstantinos Tsekouras and Prof. Steve Pressé  
Department of Physics and School of Molecular Sciences,  
Arizona State University, Tempe AZ 85287 USA

75 oSHiRLoC we combine the molecular precision 106  
 76 afforded by synthetic DNA reporters, spatial 107  
 77 information provided by fluorescence microscopy 108  
 78 and the quantitative information yielded by 109  
 79 photobleaching-based counting to map the DNase 110  
 80 II-mediated DNA processing along the 111  
 81 endolysosomal pathway.



84 **Fig 1: Work flow for counting the number of cargo DNA**  
 85 **molecules in endosomes of J774 cells.** (a) Schematic illustration  
 86 of a cell labeled with a 19:1 ratio of dsDNA-A488 (fiducial  
 87 marker) : dsDNA-Cy5 (reporter) along the endolysosomal  
 88 pathway. (b) Representative TIRF image of early endosomes (EE)  
 89 of J774A.1 cells labeled with cargo DNA cocktail imaged in  
 90 Alexa 488 channel and Cy5 channel. (c) Representative  
 91 photobleaching steps measured in Cy5 channel for the highlighted  
 92 endosome. (d) Histogram of number of photobleaching steps  
 93 observed for n = 200 lysosomes. Number of devices per  
 94 compartment = number of photobleaching steps observed ×  
 95 dilution factor.

97 In order to construct organelle specific maps of  
 98 endosomal DNA processing, we incubated (a  
 99 “pulse” step) alveolar macrophages J774A.1 cells  
 100 with a 57 base pair double-stranded (ds)DNA  
 101 reporter cargo labeled with Alexa 488 (dsDNA-  
 102 A488) in a mixture of 19:1 ratio of a reference  
 103 tracer, i.e., the same dsDNA sequence labeled with  
 104 Cy5 fluorophore (dsDNA-Cy5) (Figure 1a). Cells  
 105 were washed, incubated for a specified duration (a

106 “chase” step), fixed and imaged using total internal  
 107 reflection fluorescence (TIRF) microscopy. The  
 108 brighter, more photostable Alexa488 channel was  
 109 used as a fiducial marker of the endocytic  
 110 compartment; while the Cy5 channel was used to  
 111 generate photobleaching reporter time traces,  
 112 leveraging the low cellular autofluorescence in this  
 113 channel (Figure 1b). Given the TIRF penetration  
 114 depth of ~250 nm [29], approximately 51.66% of  
 115 early endosomes (n=6 cells), 37.34% of late  
 116 endosomes (n=5 cells) and 23.47% of lysosomes  
 117 (n=5 cells) were found to be illuminated. To  
 118 eliminate artefacts arising from autofluorescence,  
 119 only those compartments with both Alexa 488 and  
 120 Cy5 signal were analyzed. Since both DNA probes  
 121 have identical sequences, and scavenger receptors  
 122 uptake dsDNA mainly based on the overall  
 123 negative charge (17), uptake efficiency and  
 124 organelle localization is expected to be similar,  
 125 with all organelles showing similar ratios of  
 126 Cy5:Alexa488 labels (Supplementary Figure 9).  
 127 Cy5-labeled ssDNA was not retained in endosomes,  
 128 either due to its rapid degradation or endosomal  
 129 translocation.(18) This worked in our favor,  
 130 creating a clean system to report on the abundance  
 131 of dsDNA cargo which does not undergo  
 132 endosomal translocation (15). We then extracted  
 133 the number of photobleaching steps for every Cy5  
 134 time-trace (Figure 1c, Supplementary Figure 7).  
 135 The average number of DNA duplexes in a given  
 136 compartment, could then be computed from the  
 137 product of the number of photobleaching steps  
 138 observed and the probe dilution factor i.e., the ratio  
 139 of dsDNA-A488 to dsDNA-Cy5 (Figure 1d).

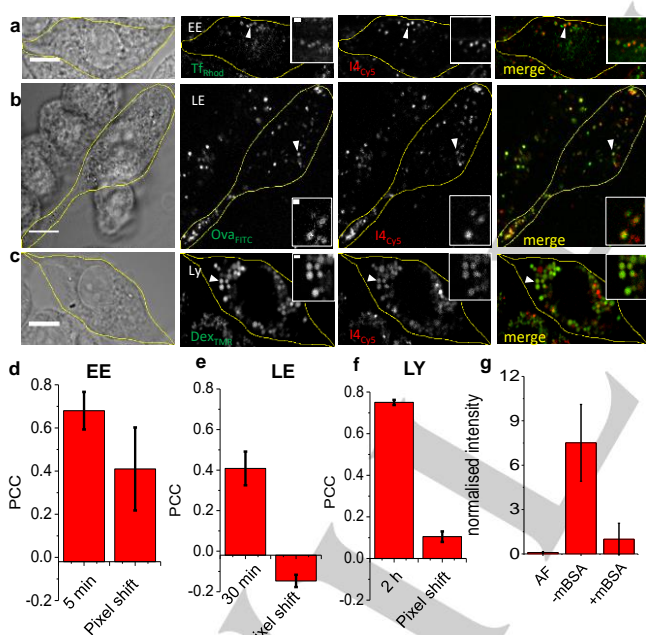
141 To assign cargo DNA molecules to specific  
 142 stages of endosomal maturation, we standardized  
 143 pulse and chase times for cargo DNA to reach the  
 144 early endosome, the late endosome and the  
 145 lysosome in J774A.1 cells. Using transferrin-  
 146 Rhodamine B as a marker for early/sorting  
 147 endosomes, (19,20) we found maximal  
 148 colocalization of transferrin-Rhodamine B (500  
 149 nM) and cargo DNA (500 nM) in early endosomes  
 150 (Figure 2a and d) and no colocalization in late  
 151 endosomes and lysosomes for a 10 min pulse  
 152 followed by a ~5-10 min chase (Supplementary  
 153 Figure 1). Similarly, ovalbumin marks late

154 endosomes in J774A.1 cells.(8) We found  
 155 significant cargo DNA colocalization with  
 156 ovalbumin-FITC with a 10 min pulse and a 30 min  
 157 chase highlighting significant localization in late  
 158 endosomes (**Figure 2b and e**) and insignificant  
 159 colocalization in early endosomes and lysosomes  
 160 (**Supplementary Figure 2**). Finally for lysosomes,  
 161 we used Dextran-TMR, which is known to mark  
 162 lysosomes in J774A.1 cells using a 16 h pulse and  
 163 a 4 h chase. Cells treated with cargo DNA and  
 164 labeled with Dextran-TMR colocalized in  
 165 lysosomes (**Figure 2c and f**) and the DNA cargo  
 166 displayed lack of colocalization in early and late  
 167 endosomes (**Supplementary Figure 3**). Next, we  
 168 established that extraneously added dsDNA was  
 169 endocytosed specifically via the scavenger receptor  
 170 (SR) pathway by using a competition assay (17).  
 171 We showed that Cy5 labeled cargo dsDNA (termed  
 172 I4<sub>Cy5</sub>) uptake was competed out by 25-fold excess  
 173 of maleylated BSA which targets SRs (**Figure 2g**).

188 (mBSA, 10  $\mu$ M) with autofluorescence control (AF). Error bars  
 189 indicate the mean of independent experiments  $\pm$  s.e.m. (n=30 cells).  
 190 Scale bars, 10  $\mu$ m and 1  $\mu$ m for inset.

191  
 192 Knowing the time-points of residence of cargo  
 193 DNA at each stage along the endolysosomal  
 194 pathway, we mapped cargo DNA abundance as a  
 195 function of endosomal maturation  
 196 (**Supplementary Figure 4**). We observed that  
 197 early endosomes showed two kinds of populations,  
 198 with endosomes containing  $\sim$ 200 or  $\sim$ 700  
 199 molecules. Overall, early endosomes showed a  
 200 mean of  $340 \pm 60$  cargo dsDNA molecules per  
 201 endosome (**Figure 3a, top panel, green line**). As  
 202 DNA is endocytosed via clathrin coated vesicles  
 203 ( $\sim$ 100 nm), we speculate the population of  
 204 endosomes showing fewer cargo DNA molecules  
 205 correspond to these smaller vesicles, while those  
 206 endosomes showing larger amounts of cargo DNA  
 207 could correspond to the larger sorting/early  
 208 endosomes. Late endosomes revealed a fairly broad  
 209 distribution of cargo DNA abundance with a mean  
 210 of  $320 \pm 80$  cargo dsDNA molecules per  
 211 compartment (**Figure 3a, middle panel, green  
 212 line**). Significantly, in lysosomes the abundance of  
 213 cargo DNA molecules showed an overall decrease,  
 214 with most compartments having a mean of  $103 \pm 7$   
 215 (**Figure 3a, bottom panel, green line**) cargo DNA  
 216 molecules, indicative of degradation or processing.

217  
 218 DNase II is known to be responsible for digestion  
 219 of endocytosed DNA in macrophages. However,  
 220 the specific endocytic organelle/s within which it is  
 221 active, is still unknown. To probe for organelle-  
 222 specific activity of DNase II in immune cells, we  
 223 treated the cells with a well-characterized specific  
 224 peptide inhibitor of DNase II, ID2-3, and  
 225 performed molecule counting experiments at each  
 226 stage of endosomal maturation (**Supplementary  
 227 Figure 5**). Upon DNase II inhibitor treatment,  
 228 counting experiments on early endosomes revealed  
 229 that the mean abundance of cargo dsDNA  
 230 molecules in early endosomes decreased to  $233 \pm 12$   
 231 upon DNase II inhibition (**Figure 3b**) suggesting a  
 232 possible slowdown of endosomal maturation but  
 233 not uptake. However, single endosome information  
 234 on cargo abundances revealed that the population  
 235 containing  $\sim$ 200 cargo dsDNA molecules had



175  
 176 **Fig 2 | Trafficking of cargo DNA along endocytic pathways.** (a)  
 177 Representative single-plane confocal images showing co-  
 178 localization of cargo with various compartment markers (a-c).  
 179 J774A.1 cells were co-pulsed with I4<sub>Cy5</sub> and (a) EE/SE marker  
 180 transferrin-Rhodamine B (Tf<sub>Rhod</sub>), (b) LE marker Ovalbumin-FITC  
 181 (Ova<sub>FITC</sub>), and (c) Lysosomal marker Dextran-TMR (Dex<sub>TMR</sub>)  
 182 followed by 2 hours chase. Cell boundaries are demarcated by  
 183 yellow outlines. (d-f) Quantification of co-localization (Pearson's  
 184 Correlation Coefficient, PCC) between cargo DNA and endosomal  
 185 markers used in a-c. Values indicate mean of n $\sim$ 20 cells. (g) I4<sub>Cy5</sub>  
 186 internalization by J774A.1 cells in the presence (+mBSA) and  
 187 absence (-mBSA) of excess competitor ligand maleylated BSA

increased at the expense of the population containing ~700 cargo dsDNA molecules ( $P$ -value  $< 0.05$ ). This suggests delayed endosomal maturation and homotypic fusion, as an overall decrease in DNA cargo due to degradation was not observed. Further, cargo DNA abundance in late endosomes (LE) was not affected by DNase II inhibition (Figure 3a, middle panel and 3b). Importantly, when we inhibited DNase II we observed a significant accumulation of undigested cargo DNA in lysosomes (Ly), showing a mean centered at  $230 \pm 80$  cargo DNA molecules (Figure 3a, bottom panel and 3b). Interestingly, our statistical data pinpoint that during DNase II inhibition, cells undergo reduced uptake/trafficking in the early endosomes (Supplementary Figure 8). This supports the current hypothesis (10) that DNase II based endosomal DNA processing occurs mainly in lysosomes (Figure 3c).

accumulation of sphingomyelin.(21) Undigested DNA in endosomes of immune cells comprises one of many important triggers of the immune response. In mice, defective digestion of chromosomal DNA activates phagocytes, leading to anaemia in the embryo and chronic arthritis in adults (22). Digestion of immunogenic CpG DNA in dendritic cells showed that endosomally localized DNase II activity is necessary to trigger TLR-9 mediated cytokine production.(4) Loss of DNase II activity results in autoimmune disorders such as systemic lupus erythematous, for which, one of the hallmarks is the production of autoantibodies against dsDNA.(22,23) Our capacity to model the immune response using predictive computational models has been hindered by our inability to accurately specify the location and abundance of ligands such as dsDNA that trigger the immune response. The endosomal load of unprocessed dsDNA cargo is a function of the rate of endocytosis, concentration of exogenous dsDNA, receptor density on plasma membrane and organelle-specific DNase II activity along the endolysosomal pathway.(4,24) Current methods to analyze DNA processing quantitate processing efficiency albeit without organelle-specific information, or organelle-specific information without the ability to quantitate processing. (25)

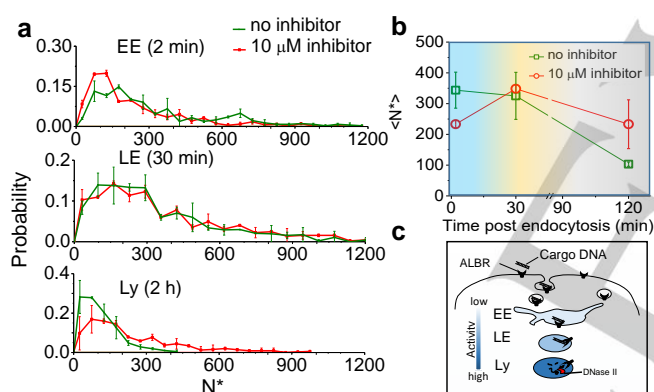


**Fig 3: Quantitative maps of endosomal DNA processing by single molecule counting.** (a) Histograms of number of DNA devices observed per compartment in early endosomes (EE, 2 min post endocytosis), late endosomes (LE, 30 min post endocytosis) and lysosomes (Ly, 2h post endocytosis) in presence and absence of 10  $\mu$ M DNase II inhibitor within J774A.1 cells. (b) Average number of DNA devices per compartment as a function of time. Blue shade indicates EE, orange indicates LE while grey corresponds to Ly. Total number of devices per compartment ( $*N$ ) = number of photobleaching steps observed  $\times$  dilution factor.  $n = 200$  endosomes (duplicate) (c) Proposed model of DNase II activity in endosomes.

Further, delayed endosomal maturation as a result of cargo accumulation in lysosomes is also observed in the context of several lysosomal storage disorders e.g., trafficking of acid sphingomyelinase (ASM) to the lysosome is impeded in ASM knock out cells due to lysosomal

oSHiRLoC provides quantitative information on cargo DNA processing at an organellar resolution. Endosomal cargo quantification using oSHiRLoC is not limited to dsDNA, and can be applied to a range of externally added endocytic ligands. It can also be used to assay the location and activity of regulators of endosomal cargo processing. Given the burgeoning use of biologically active, synthetic DNA and RNA nanostructures, circulating endogenous DNA and RNA molecules, methods to understand their differential processing within the cell would be critical to uncover their mechanisms of action. The ability to determine the concentration of immunogens in specific endocytic organelles and correlate these with the strength of the downstream immune response would enable us to quantitatively model the immune response.

324 **Acknowledgements**

325 We thank Shareefa Thekkan, Kasturi Chakraborty,  
326 Junyi Zou, Aditya Prakash and Vytas Bindokas for  
327 technical assistance and code optimization and  
328 Research Computation Center (RCC), and the  
329 University of Chicago for providing computational  
330 infrastructure. V.P. thanks Dr. Sethuramasundaram  
331 Pitchiaya, Damon Hoff and Elizabeth Cameron for  
332 initial training and U Chicago for funding. K.T.  
333 thanks S.Jazani for his help in testing the software.  
334 J774A.1 cells were a kind gift from Prof. Deborah  
335 Nelson, Department of Pharmacological and  
336 Physiological Sciences, the University of Chicago.

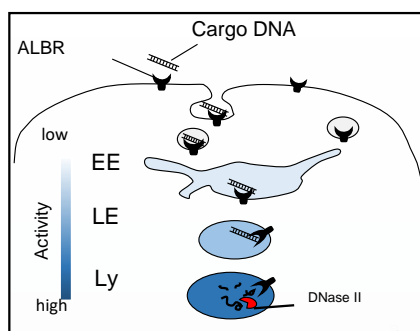
337  
338 **Keywords:** DNA, single molecule counting,  
339 oSHiRLoC, endosomal maturation,  
340 photobleaching, DNase II, quantitative biology,  
341 lysosome

- 342  
343 1. Rincon-Restrepo M, Mayer A, Hauert S, Bonner DK, Phelps EA,  
344 Hubbell JA, et al. Vaccine nanocarriers: Coupling intracellular  
345 pathways and cellular biodistribution to control CD4 vs CD8 T cell  
346 responses. *Biomaterials*. 2017 Jul;132:48–58.
- 347 2. Barton GM, Kagan JC, Medzhitov R. Intracellular localization of  
348 Toll-like receptor 9 prevents recognition of self DNA but  
349 facilitates access to viral DNA. *Nat Immunol*. 2006 Jan;7(1):49–  
350 56.
- 351 3. Compeer EB, Flinsenbergh TWH, van der Grein SG, Boes M.  
352 Antigen processing and remodeling of the endosomal pathway:  
353 requirements for antigen cross-presentation. *Front Immunol*. 2012  
354 Mar 7;3:37.
- 355 4. Chan MP, Onji M, Fukui R, Kawane K, Shibata T, Saitoh S, et al.  
356 DNase II-dependent DNA digestion is required for DNA sensing  
357 by TLR9. *Nat Commun*. 2015 Jan 20;6:5853.
- 358 5. Amessou M, Popoff V, Yelamos B, Saint-Pol A, Johannes L.  
359 Measuring retrograde transport to the trans-Golgi network. *Curr*  
360 *Protoc Cell Biol*. 2006 Oct;Chapter 15:Unit 15.10.
- 361 6. Weihe A. Quantification of organellar DNA and RNA using real-  
362 time PCR. *Methods Mol Biol*. 2014;1132:235–243.
- 363 7. Sperinde JJ, Choi SJ, Szoka FC. Phage display selection of a  
364 peptide DNase II inhibitor that enhances gene delivery. *J Gene*  
365 *Med*. 2001 Apr;3(2):101–108.
- 366 8. Tjelle TE, Brech A, Juvet LK, Griffiths G, Berg T. Isolation and  
367 characterization of early endosomes, late endosomes and terminal  
368 lysosomes: their role in protein degradation. *J Cell Sci*. 1996  
369 Dec;109 ( Pt 12):2905–2914.
- 370 9. Qian Z, Dougherty PG, Pei D. Monitoring the cytosolic entry of  
371 cell-penetrating peptides using a pH-sensitive fluorophore. *Chem*  
372 *Commun (Camb)*. 2015 Feb 7;51(11):2162–2165.
- 373 10. Evans CJ1, Aguilera RJ. DNase II: genes, enzymes and  
374 function. *Gene*. 2003 Dec 11;322:1–15.
- 375 11. Brown JA, Swank RT. Subcellular redistribution of newly  
376 synthesized macrophage lysosomal enzymes. Correlation between  
377 delivery to the lysosomes and maturation. *J Biol Chem*. 1983 Dec  
378 25;258(24):15323–15328.
- 379 12. Yang J, Chen H, Vlahov IR, Cheng J-X, Low PS. Evaluation of  
380 disulfide reduction during receptor-mediated endocytosis by using  
381 FRET imaging. *Proc Natl Acad Sci U S A*. 2006 Sep  
382 12;103(37):13872–13877.
- 383 13. Puchner EM, Walter JM, Kasper R, Huang B, Lim WA. Counting  
384 molecules in single organelles with superresolution microscopy  
385 allows tracking of the endosome maturation trajectory. *Proc Natl*  
386 *Acad Sci U S A*. 2013 Oct 1;110(40):16015–16020.
- 387 14. Jungmann R, Avendaño MS, Dai M, Woehrstein JB, Agasti SS,  
388 Feiger Z, et al. Quantitative super-resolution imaging with  
389 qPAINT. *Nat Methods*. 2016 May;13(5):439–442.
- 390 15. Tsekouras K, Custer TC, Jashnsaz H, Walter NG, Pressé S. A  
391 novel method to accurately locate and count large numbers of steps  
392 by photobleaching. *Mol Biol Cell*. 2016 Nov 7;27(22):3601–3615.
- 393 16. Pitchiaya S, Heinicke LA, Park JI, Cameron EL, Walter NG.  
394 Resolving Subcellular miRNA Trafficking and Turnover at Single-  
395 Molecule Resolution. *Cell Rep*. 2017 Apr 18;19(3):630–642.
- 396 17. Modi S, M G S, Goswami D, Gupta GD, Mayor S, Krishnan Y. A  
397 DNA nanomachine that maps spatial and temporal pH changes  
398 inside living cells. *Nat Nanotechnol*. 2009 May;4(5):325–330.
- 399 18. Lorenz S, Tomcin S, Mailänder V. Staining of mitochondria with  
400 Cy5-labeled oligonucleotides for long-term microscopy studies.  
401 *Microsc Microanal*. 2011 Jun;17(3):440–445.
- 402 19. Raje CI, Kumar S, Harle A, Nanda JS, Raje M. The macrophage  
403 cell surface glyceraldehyde-3-phosphate dehydrogenase is a novel  
404 transferrin receptor. *J Biol Chem*. 2007 Feb 2;282(5):3252–3261.
- 405 20. Wadsworth SJ, Goldfine H. Mobilization of protein kinase C in  
406 macrophages induced by *Listeria monocytogenes* affects its  
407 internalization and escape from the phagosome. *Infect Immun*.  
408 2002 Aug;70(8):4650–4660.
- 409 21. Dhami R, Schuchman EH. Mannose 6-phosphate receptor-  
410 mediated uptake is defective in acid sphingomyelinase-deficient  
411 macrophages: implications for Niemann-Pick disease enzyme  
412 replacement therapy. *J Biol Chem*. 2004 Jan 9;279(2):1526–1532.
- 413 22. Kawane K, Fukuyama H, Kondoh G, Takeda J, Ohsawa Y,  
414 Uchiyama Y, et al. Requirement of DNase II for definitive  
415 erythropoiesis in the mouse fetal liver. *Science*. 2001 May  
416 25;292(5521):1546–1549.
- 417 23. Kawane K, Motani K, Nagata S. DNA degradation and its defects.  
418 *Cold Spring Harb Perspect Biol*. 2014 Jun 2;6(6).
- 419 24. Scott CC, Vacca F, Gruenberg J. Endosome maturation, transport  
420 and functions. *Semin Cell Dev Biol*. 2014 Jul;31:2–10.
- 421 25. Hiroi N, Draviam VM, Funahashi A. Editorial: quantitative  
422 biology: dynamics of living systems. *Front Physiol*. 2016 Jun  
423 2;7:196.
- 424 26. Dunn KW1, Kamocka MM, McDonald JH. A practical guide to  
425 evaluating colocalization in biological microscopy. *Am J Physiol*  
426 *Cell Physiol*. 2011 Apr;300(4):C723–42.
- 427 27. Surana S, Bhat J M, Koushika S P & Krishnan Y. An autonomous  
428 DNA nanomachine maps spatiotemporal pH changes in a  
429 multicellular living organism. *Nature Communications* 2011  
430 volume 2, Article number: 340
- 431 28. Lyon C.J., Evans C.J., Bill B.R., Otsuka A.J., Aguilera R.J.  
432 The *C. elegans* apoptotic nuclease NUC1 is related in sequence and  
433 activity to mammalian DNase II. *Gene*, 252 (2000), pp. 147–154
- 434 29. Fish K N. Total Internal Reflection Fluorescence (TIRF)  
435 Microscopy. *Curr Protoc Cytom*. 2009 Oct; 0 12: Unit12.18.
- 436 30. Kim J, Choi D-K, Park S, Shin S-M, Bae J, Kim D-M, et al.  
437 Quantitative assessment of cellular uptake and cytosolic access of  
438 antibody in living cells by an enhanced split GFP complementation  
439 assay. *Biochem Biophys Res Commun*. 2015 Nov 27;467(4):771–  
440 777.
- 441 31. Narayanaswamy N, Chakraborty K, Saminathan A, Zeichner E,  
442 Leung K, Devany J & Krishnan Y. A pH-correctable, DNA-based  
443 fluorescent reporter for organellar calcium. *Nature Methods*  
444 volume 16, pages95–102 (2019)
- 445 32. Shareefa Thekkan, Maulik S. Jani, Chang Cui, Krishna Dan,  
446 Guolin Zhou, Lev Becker & Yamuna Krishnan. A DNA-based  
447 fluorescent reporter maps HOC1 production in the maturing  
448 phagosome. *Nature Chemical Biology* (2018)

1

## COMMUNICATION

Text for Table of Contents



*Ved Prakash, Konstantinos Tsekouras, Muthukumar Venkatachalapathy, Laurie Heineke, Steve Pressé, Nils G. Walter\* & Yamuna Krishnan\**

**Page No. – Page No.**

**Quantitative maps of endosomal DNA processing by single molecule counting**

2

3

4

5